Terahertz particle-in-liquid sensing with spoof surface plasmon polariton waveguides

Ma, Zhijie; Hanham, Stephen

DOI:
10.1063/1.4998566

Document Version
Publisher's PDF, also known as Version of record

Citation for published version (Harvard):
Ma, Z & Hanham, S 2017, 'Terahertz particle-in-liquid sensing with spoof surface plasmon polariton waveguides', *APL Photonics*, vol. 2, 116102. https://doi.org/10.1063/1.4998566

Terahertz particle-in-liquid sensing with spoof surface plasmon polariton waveguides

Zhijie Ma, Stephen M. Hanham, Paloma Arroyo Huidobro, Yandong Gong, Minghui Hong, Norbert Klein, and Stefan A. Maier

Citation: APL Photonics **2**, 116102 (2017);
View online: https://doi.org/10.1063/1.4998566
View Table of Contents: http://aip.scitation.org/toc/app/2/11
Published by the American Institute of Physics

Terahertz particle-in-liquid sensing with spoof surface plasmon polariton waveguides

Zhijie Ma,[1,2,3] Stephen M. Hanham,[4] Paloma Arroyo Huidobro,[1] Yandong Gong,[3] Minghui Hong,[3] Norbert Klein,[4] and Stefan A. Maier[1,a]
[1]*Department of Physics, Imperial College London, London SW7 2AZ, United Kingdom*
[2]*NUS Graduate School for Integrative Sciences and Engineering (NGS), National University of Singapore, Singapore 117456, Singapore*
[3]*Department of Electrical and Computer Engineering, National University of Singapore, Singapore 117576*
[4]*Department of Materials, Imperial College London, London SW7 2AZ, United Kingdom*

(Received 1 August 2017; accepted 8 October 2017; published online 26 October 2017)

We present a highly sensitive microfluidic sensing technique for the terahertz (THz) region of the electromagnetic spectrum based on spoof surface plasmon polaritons (SPPs). By integrating a microfluidic channel in a spoof SPP waveguide, we take advantage of these highly confined electromagnetic modes to create a platform for dielectric sensing of liquids. Our design consists of a domino waveguide, that is, a series of periodically arranged rectangular metal blocks on top of a metal surface that supports the propagation of spoof SPPs. Through numerical simulations, we demonstrate that the transmission of spoof SPPs along the waveguide is extremely sensitive to the refractive index of a liquid flowing through a microfluidic channel crossing the waveguide to give an interaction volume on the nanoliter scale. Furthermore, by taking advantage of the insensitivity of the domino waveguide's fundamental spoof SPP mode to the lateral width of the metal blocks, we design a tapered waveguide able to achieve further confinement of the electromagnetic field. Using this approach, we demonstrate the highly sensitive detection of individual sub-wavelength micro-particles flowing in the liquid. These results are promising for the creation of spoof SPP based THz lab-on-a-chip microfluidic devices that are suitable for the analysis of biological liquids such as proteins and circulating tumour cells in buffer solution. https://doi.org/10.1063/1.4998566

I. INTRODUCTION

The terahertz (THz) region of the electromagnetic spectrum, lying between microwaves and infrared light, is an important band for sensing due to its non-ionizing nature and the many intermolecular vibrational and rotational modes of polar molecules present. One area where THz sensing is predicted to have a significant impact is in biological sensing,[1,2] particularly, bio-liquids such as aqueous solutions of proteins, DNA, and cells. The use of THz waves in these applications is hindered by its relatively long wavelength compared with the size of the sample to be characterised. Therefore, techniques which enhance light-matter interactions in the THz regime through strong confinement of the electromagnetic field are highly desirable.[3]

One approach to achieve this is to use metamaterials consisting of periodic metallic or dielectric resonators in which the localized electromagnetic fields are strongly enhanced.[4–8] A successful alternative has been to borrow the ideas of surface plasmon polaritons (SPPs) from the visible and near-infrared regions. The past few years have witnessed the rapid growth of research in plasmonics for its capability to provide strong field confinement and its high sensitivity to environmental

[a]Electronic mail: s.maier@imperial.ac.uk

refractive index changes.[9] However, in the terahertz frequency band, the high conductivity of metals only allows for poorly confined Sommerfeld-Zenneck waves to propagate on their surfaces. To overcome this, Pendry *et al.* proposed the use of structured metal surfaces with holes in them to mimic the SPPs that appear in the visible regime but at much lower frequencies,[10,11] as was experimentally verified by Hibbins *et al.*[12–14] These surface waves are termed spoof or "designer" surface plasmon polaritons. Since then, spoof SPPs have been extensively studied for the confined waveguiding of THz electromagnetic waves in various situations.[15–23] Spoof SPPs can be excited by matching their momentum to free-space radiation using the edge coupling method[13] or through a tapered mode converter to couple with conventional waveguides or transmission lines.[17,24–26] In addition, the localized version of spoof surface plasmons can also be excited in closed geometries, and subwavelength electric and magnetic dipolar resonances have been demonstrated.[27,28] Recent researches have also shown that, in the mid-infrared and terahertz frequencies, surface plasmon can be excited and propagated on two-dimensional materials such as graphene and single-layer black phosphorus, in which the free carrier density can be tuned by chemical doping or electrical gating.[29–31]

The most commonly employed spoof SPP platforms consist of corrugated metal surfaces or waveguide geometries,[11,32–34] including ultrathin waveguides.[16,17,21,35] In these designs, the optical properties of the spoof surface or waveguide can be readily controlled by the geometrical parameters. Spoof SPP waves can confine electromagnetic energy on subwavelength scales, greatly enhancing light-matter interaction with the local dielectric environment. In the THz regime, spoof SPPs provide the advantage of shrinking the relatively long wavelength of THz waves to a subwavelength scale comparable with the dimension of biological analyte targets. All these properties, together with the capability of guiding electromagnetic energy with spoof SPP waveguides, provide a new operating principle for optofluidic sensors, which combine the advantages of compact and rapid handling of microfluidics and the high detection sensitivity of the optical analysis. So far, a variety of waveguide-based optofluidic sensors have been demonstrated, including resonant microcavities,[36,37] photonic crystal resonators,[38] interferometer waveguide,[39] and others.[6,40–43] Spoof surfaces as THz sensing platforms have been experimentally demonstrated for sensing both the real and imaginary parts of the refractive index of certain materials.[44–46] However, these sensing schemes operate with all of the grooves filled with the sample analyte, which may not be feasible for many situations where only a small volume of sample liquid is available. Moreover, the liquids are also not well guided, making integration with microfluidics for lab-on-chip sensing devices difficult.

In this paper, we demonstrate a microfluidic sensing platform consisting of a spoof SPP domino waveguide[34,47,48] and a micro-capillary through which a liquid sample can be introduced into the spoof SPP's field. We show through numerical simulations that high sensitivity detection of the refractive index of liquids can be achieved in the THz range. When the refractive index of the liquid inside the capillary is changed, a significant shift in the transmission spectrum of the spoof SPP waves occurs. The small interaction area between the micro-capillary and the spoof SPP mode, which is, in particular, determined by the lateral dimension of the waveguide, implies that a liquid volume only in the nanoliter scale is required. Furthermore, by using a tapered design with a gradually narrowing lateral block width, spoof SPP waves can be further confined in the lateral direction, making it possible to detect single micro-particles with diameters significantly smaller than the radiation wavelength passing through the capillary. The proposed sensing platform has the advantage that the liquid samples are completely contained in the microfluidic system, which can be useful for integrated lab-on-chip sensing devices in the future.

II. THEORY AND MODEL

The schematics of the two proposed spoof SPP waveguide optofluidic sensors are shown in Fig. 1. The waveguide consists of an array of periodic metallic blocks standing on a metal surface, and a micro-capillary is positioned through one of the grooves, with its center at the same height as the top of the domino blocks. The geometrical parameters of the domino blocks are denoted in the inset figure which shows the transverse cross section of the waveguide. The quartz capillary

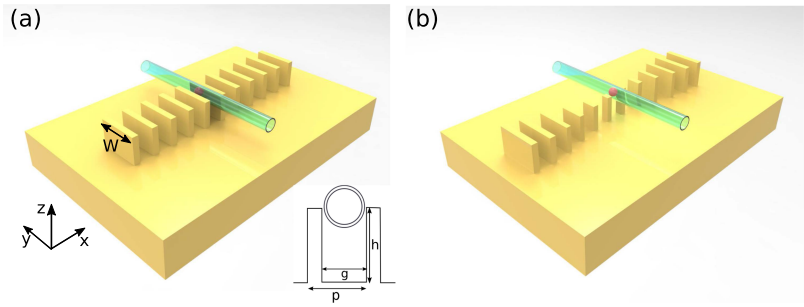

FIG. 1. Schematics of the homogeneous (a) and the tapered (b) spoof SPP domino waveguides, with lateral width W, period p, groove depth h, and groove gap width g as indicated in the inset figure. A micro-capillary is positioned in the center groove. The center of the capillary is aligned with the top of the domino blocks.

has an outer diameter of 130 μm, a wall thickness of 10 μm, and a constant permittivity of 3.8. The homogeneous domino waveguide in Fig. 1(a) has periodic blocks of the same lateral width W. The tapered domino, sketched in Fig. 1(b), features a domino width that decreases slowly from the neighbour block, and the capillary is positioned at the center of the waveguide where W is narrowest. Experimentally, the domino blocks may be fabricated by deep reactive ion etching (DRIE) of silicon[4] or 3D printing of polymers[49] followed by metal deposition. In the THz regime, the skin depth of gold is very small compared with the wavelength of radiation, and the ohmic loss is very small. For simplicity, the metal is assumed to be a perfect electric conductor in all the simulations.

We start by considering the dispersion relation of the spoof SPP modes that propagate on a domino waveguide. The dispersion relations are calculated using the finite element method (FEM) in COMSOL Multiphysics. In Fig. 2(a), the calculated dispersion curves are plotted for different values of W and the two-dimensional case which corresponds to $W \to \infty$, with other

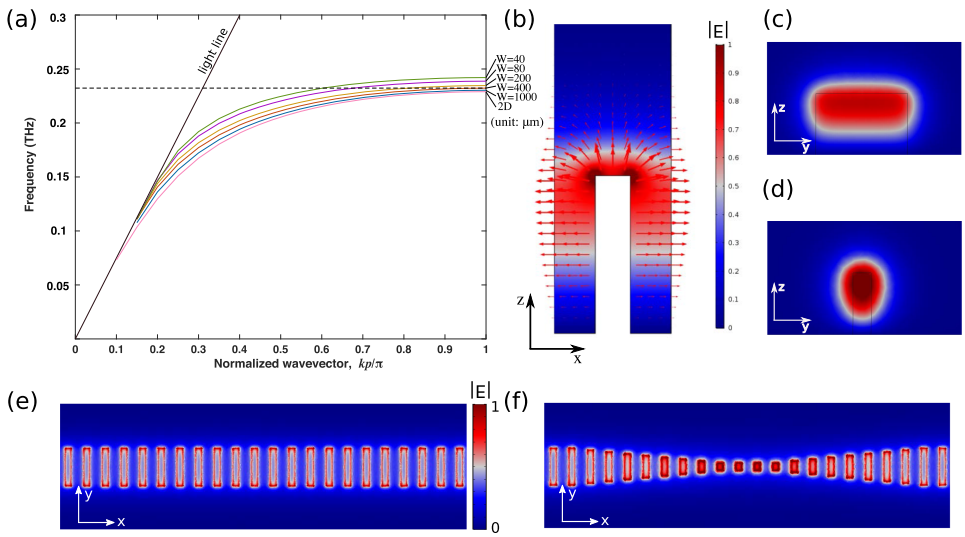

FIG. 2. (a) Dispersion curve of the spoof SPP modes for domino blocks with different lateral widths W = 40 μm, 80 μm, 200 μm, 400 μm, and 1000 μm, with other geometrical parameters fixed as p = 200 μm, h = 270 μm, and g = 140 μm. The 2D line corresponds to infinitely wide domino ($W \to \infty$), and the light line is indicated with a solid black line. The dashed line marks the cutoff frequency of the spoof SPP for W = 400 μm. The normalized electric field distribution of the spoof SPP wave from (b) xz-plane and yz-plane with (c) W = 400 μm and (d) W = 80 μm. Normalized electric intensity at the plane of the domino top for (e) the homogeneous waveguide and (f) the tapered waveguide. The width of the homogeneous domino waveguide is W = 400 μm, for the tapered waveguide, the domino blocks start from W = 400 μm and decrease in 40 μm step to W = 80 μm.

geometry parameters fixed as $p = 200\ \mu$m, $h = 270\ \mu$m, and $g = 140\ \mu$m [see the inset of Fig. 1(a)]. k denotes the wavenumber of spoof SPP waves propagating in the x-direction, and it is normalized to the maximum value π/p. The modes that are below the light-line are confined non-radiative modes. For larger k values, the deviation from the light-line is greater and the mode is more confined to the surface, propagating at a slower group velocity.[19] The dispersion relation for an infinitely wide domino array, i.e., a spoof surface, can be analytically approximated by[15,34,50]

$$k = k_0\sqrt{1 + \frac{g^2}{p^2}\tan^2(k_0 h)}, \tag{1}$$

where k_0 is the wavenumber of free space radiation. From the equation, one can see that the asymptotic frequency of the spoof SPP mode is mainly determined by the groove depth h. Deep grooves allow for the emergence of higher order modes in the vertical direction inside the grooves,[50] and in this paper, we concentrate only on the first order mode. In the three-dimensional case with finite lateral width W, it was previously demonstrated that the dispersion relation of spoof SPPs on domino blocks is relatively insensitive to the lateral width W.[34] In Fig. 2(a), we see that the asymptotic frequencies only change slightly with significantly different lateral widths. For $W = 400\ \mu$m, the asymptotic frequency equals to 0.23 THz, and it is indicated with a dashed line parallel to the x axis. With smaller lateral width, the asymptotic frequency increases, and the overall spoof SPP mode appears to be less confined from the dispersion curve; however, the electric fields are more concentrated in the lateral y-direction due to the reduction in that dimension. In Fig. 2(b), the normalized electric (E)-field intensity and the E-field vectors at the asymptotic frequency are plotted in the transverse cross section (xz-plane). From the electric near-field distribution, we can see that the field intensity is most concentrated at the top of the domino, and the field decays exponentially away from that interface, similar to a conventional surface plasmon mode. In order to maximize the interaction between the liquid and the spoof SPP wave, the capillary is aligned with the top of the domino where the field enhancement is the greatest.

In Figs. 2(c) and 2(d), the normalized E-field distributions are plotted on the yz-plane at the middle of the grooves for widths $W = 400\ \mu$m and $W = 80\ \mu$m, showing more concentrated electric field for narrower domino width. Figures 2(c) and 2(e) both show that, in the lateral y-direction, the field intensity is relatively constant except for the hotspots at the block corners. It should be noted that in the domino structures with large lateral width, higher order transverse modes with varying charge distribution in the lateral direction are supported. These modes can have anti-nodes with zero field intensity in the center,[47] which is not beneficial for our purpose and we do not discuss them further in this paper.

For the simulation of the transmission behavior of the domino waveguide, an electric dipole oscillating in the x-direction is positioned at the beginning of the dominoes to excite the spoof SPP mode. Two-plane field monitors integrating the Poynting vector of the spoof SPP waves are set apart with a distance of 40 periods of dominoes. The transmission rate is calculated by normalizing the power integrated on the farther plane from the dipole to that from the nearer plane. In Fig. 2(e), the normalized E-field intensity on the homogeneous domino waveguide ($W = 400\ \mu$m) without the capillary is plotted. This figure shows that the E-field amplitude remains constant over the dominoes, suggesting that there is no radiation or reflection loss along propagation. In contrast, the E-field amplitude for the tapered waveguide is plotted in Fig. 2(f), showing field enhancement in the center. In the study, the lateral width of the tapered domino waveguide starts at $W = 400\ \mu$m and decreases in steps of $40\ \mu$m to the narrowest width of $W = 80\ \mu$m, with an array of 4 domino blocks with constant W = $80\ \mu$m at the center. From Fig. 2(a), we observe that the domino with smaller lateral width has slightly higher cutoff frequency than the large width domino. Therefore, a tapered domino waveguide with slowly decreasing lateral width can support gradually confined spoof SPP waves without significant propagation loss. We can observe in Fig. 2(f) that in this tapered waveguide, the fields are more confined in the center region with smaller cross section, and it is expected that light-matter interaction between the SPP wave and the analyte will be enhanced in this region.

III. RESULTS AND DISCUSSION

In this section, we demonstrate how a change in the refractive index of liquid flowing through the micro-capillary or a single micro-particle passing through it affects the transmission of the spoof SPP waves on the domino waveguide, which can be used for sensing applications. The basic structures of the waveguide sensor are as shown in Fig. 1. First, we consider sensing of homogeneous liquids flowing through the micro-capillary channel [see Fig. 1(a)]. Liquids with different refractive indices are pumped through the capillary, and the transmission spectrum is measured for each case. In the simulation, the tested materials correspond to nitrogen (n = 1), gasoline (n = 1.4), liquid paraffin (n = 1.5), glycerin (n = 1.82), and glucose (n = 2.1),[6,44] neglecting losses. In Fig. 3(a), the transmission (T) spectra for a domino waveguide (W = 400 μm) with different liquids in the capillary are plotted. It is shown that when no capillary is inserted, the spoof SPP wave can propagate on the waveguide with nearly no radiative loss over the propagation band, maintaining a high transmission rate over 90%, until it meets the cutoff frequency of 0.23 THz where no spoof SPP mode can propagate. In the presence of a liquid-filled capillary, the transmissions start to drop at frequencies lower than the cut-off frequency of the domino waveguide, and the higher the index of the liquid, the more redshifted the transmission cutoff frequency is. This way, the transmission spectrum reflects changes in the refractive index value. These results demonstrate liquid sensing at THz frequencies with spoof SPPs using only a single groove, with greatly reduced interaction volume on the nanoliter scale. Such a small interaction volume also provides the advantage of preventing the transmitted signal from being completely attenuated by the high absorption of some lossy liquids in THz such as water.

To explore why the domino waveguide sensor has such high sensitivity to the index change in one of the grooves, we performed an eigenfrequency study for the unit domino structure with the capillary filled with materials of different refractive index. The dispersion curves of the spoof SPP mode are

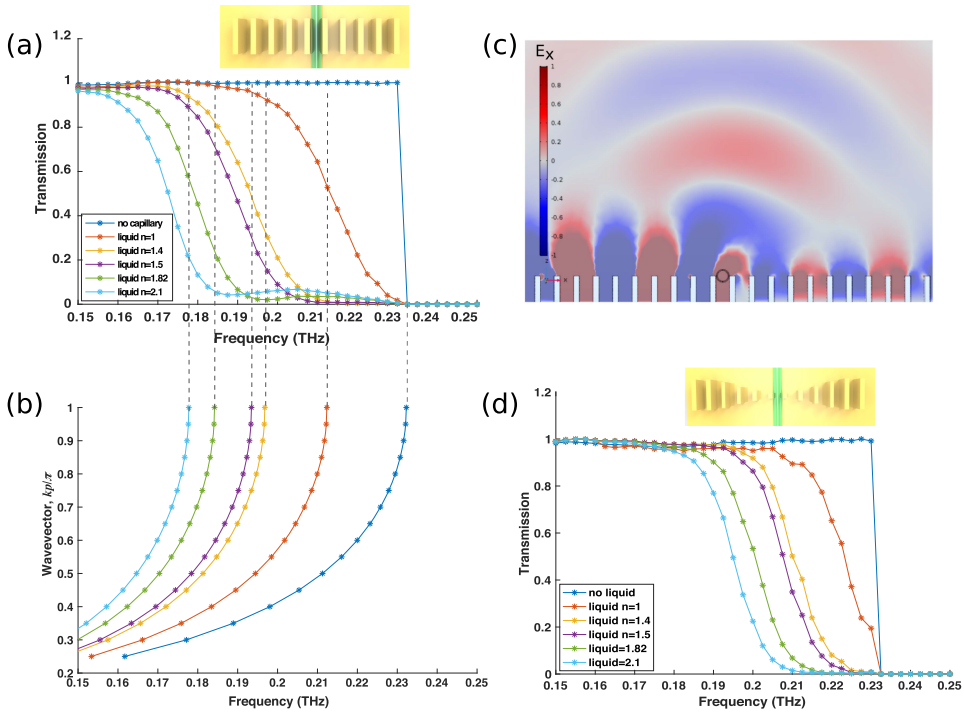

FIG. 3. (a) Transmission spectra for a homogeneous domino waveguide without and with a liquid-filled capillary. The capillary has an inner diameter of 110 μm and an outer diameter of 130 μm. The liquid refractive indices are set to be 1, 1.4, 1.5, 1.82, and 2.1. (b) The dispersion curves of the domino waveguide with capillary and liquids of refractive indices stated in (a). (c) The near-field of E_x at f = 0.21 THz, showing the field scattered by the capillary and the reduced electric field amplitude in the transmitted spoof SPP wave. (d) The transmission spectra for a tapered domino waveguide with the same liquid refractive indices as in (a).

plotted in Fig. 3(b). The dashed lines connecting Figs. 3(a) and 3(b) serve as a guide for the eye to show the connection between the cut-off frequencies of the spoof SPP modes and the corresponding reduction in the transmission of the domino waveguide with filled capillary. As shown in the figure, the higher the refractive index inside the capillary, the lower the cut-off frequency of the spoof SPP mode is because the presence of the capillary and liquids increases the average refractive index in the groove, effectively increasing the groove cavity length. From Figs. 3(a) and 3(b), one can see that the cutoff frequency of a groove with capillary is closely related to the frequency point where the transmission of the domino waveguide reduces to $1/e$. As the liquid refractive index increases, the cut-off frequency of the groove decreases and the transmission spectrum displays a low-pass behavior with a lower cut-off frequency. In the lower frequency region of the transmission spectrum, the mode is less confined, with the spoof SPP wavelength being much larger than the capillary size. Therefore, the spoof SPP waves can pass around the capillary without too much scattering or reflection and the transmission rate is kept close to one, independent of the liquid refractive index. However, it should be pointed out that because the properties of only one groove are changed by the presence of the capillary, its effect is similar to scattering from a defect in a periodic structure. A complete transmission-forbidden bandgap is not formed, and spoof SPP waves can tunnel through the defect barrier and propagate along the waveguide. This explains why the transmission drop is not sharp as in the case of a domino waveguide without the capillary [see dark blue line in Fig. 3(a)]. To observe the effect of the capillary on the spoof SPP waves, we plot in Fig. 3(c) the near-field of the instantaneous x-component of the electric field on the homogeneous waveguide with capillary, with $k = 0.5$, and $f = 0.21$ THz, in the xz viewing plane. It can be seen that part of the spoof SPP field is scattered by the capillary and radiated into free space, and the transmitted spoof SPP wave has a greatly reduced amplitude.

The sensitivity of the system can be characterized by $S = \frac{\partial T}{\partial n}$ at a given frequency and liquid refractive index n, where T is the power transmission rate. In the homogeneous waveguide sensor, the maximum S has a value of 1.89/RIU at 0.19 THz. In Fig. 3(d), we show the transmission spectra for the tapered domino waveguide with the same liquids as in homogeneous waveguide. Overall, it shows the same trend as in the homogeneous domino waveguide, the transmission cut-off redshifts with increasing liquid refractive index. However, the shift is less significant compared to that in the homogeneous waveguide, and the sensitivity is also weaker with a calculated value of 1.54/RIU. The reduced performance in the tapered waveguide sensor for the liquid index change can be explained by the smaller interaction volume with the liquids due to the reduction in the lateral y-direction, and the fact that the slight rise of the cut-off frequency with smaller W also results in lower confinement of the spoof SPP waves in the z-direction.

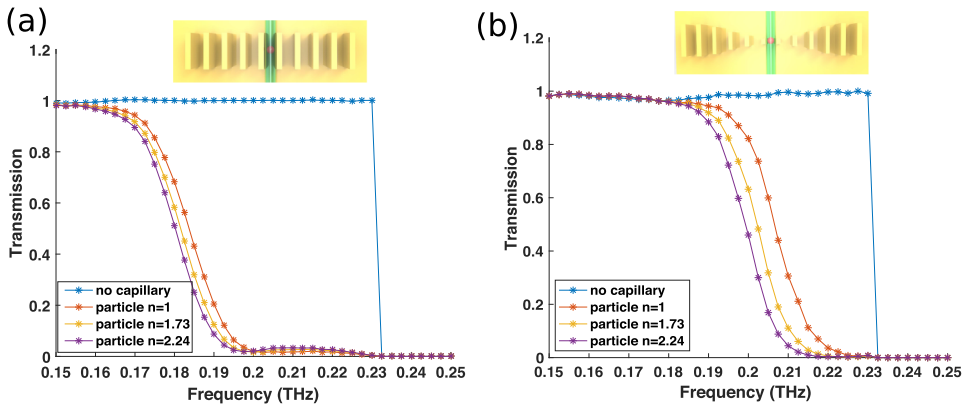

FIG. 4. Sensing a single micro-particle passing through the capillary. (a) Transmission spectra of a homogeneous domino waveguide with a single spherical particle in a liquid inside the capillary. The particle, with diameter 90 μm, is positioned at the center of the groove, and its refractive index takes values of $n = 1$, 1.73, 2.24. The background liquid in the capillary $n = 1.73$. (b) Transmission spectra for the tapered domino waveguide with capillary and particle, with particle parameters being the same as in (a).

Now we discuss the performance of these two domino waveguide sensors for the detection of a sub-wavelength micron-sized particle passing through the capillary. In the simulations, a particle with diameter d = 90 μm is positioned at the center of the capillary, and the background liquid is set to have refractive index of 1.73. The transmission spectra for particles with different index values of 1, 1.73, and 2.24 are calculated and plotted in Fig. 4 for the homogeneous and the tapered domino waveguide sensors. By comparing the two plots, it can be seen that the tapered design has higher sensitivity than the homogeneous waveguide for detection of single micron sized particles, with sensitivity being improved from 0.15/RIU in the homogeneous waveguide to 0.35/RIU in the tapered design. In the homogeneous domino waveguide, the ratio of the particle volume to the whole spoof SPP-liquid interaction volume is rather small, so the change in the index of the particle does not result in a significant shift in the spoof SPP transmission spectra. In comparison, at the center of the tapered waveguide, where the cross section is narrowest (80 μm), the mode is squeezed in the lateral direction into a scale comparable with the particle's diameter, which makes the transmission more sensitive to the change of the particle index. Remarkably, at 0.2 THz, the free space wavelength is $\lambda_0 \sim 1500$ μm, which is substantially larger than the particle's diameter, of only 90 μm. However, as we have shown, the enhanced field and wavelength shrinking provided by the spoof SPP enables sub-wavelength detection of the micro-particle with high sensitivity.

Finally, we note that in the discussion above, the liquids and domino waveguide materials have been assumed to be lossless. In practice, the materials will exhibit some loss and this will lead to the attenuation of the transmission signal, particularly near the cut-off frequency due to the tight confinement of the spoof SPP mode. For example, in our target frequency, based on the double Debye model, water has a high imaginary part of refractive index around 1–2, which will significantly attenuate the signal. A careful balance between the sensitivity and the tolerable loss needs to be optimized in this case. We suggest that one possible way to control the level of interaction between the spoof SPP waves and lossy analytes is by changing the vertical position of the capillary or operating at a frequency with a lower level of confinement. However, we stress that while materials are assumed to be lossless for simplicity, the operating principle and mechanism can be applied to realistic situations.

IV. CONCLUSION

In summary, we have numerically demonstrated a domino waveguide microfluidic sensor in the THz regime, where the spoof SPP modes can tightly confine THz waves. This greatly enhances light-matter interaction with the analytes in the capillary in a single groove. The transmission spectrum of the spoof SPP wave is highly sensitive to the refractive index of the analyte, which is on the scale of nanoliters, providing a new method for waveguide-based optofluidic sensing. Furthermore, by exploiting the insensitivity of the spoof SPP on the width of the domino blocks, the tapered domino waveguide with slowly shrinking width can greatly squeeze the spoof SPP mode into a narrower region with better field concentration, making it more promising for the detection of a sub-wavelength micro-particle. We have shown that the high sensitivity is due to the high refractive index liquid or particle decreasing the cut-off frequency of the spoof SPP mode in one groove, resulting in a significant reduction in transmission of the spoof SPP waves through this waveguide section. These findings can be of value for integrated microfluidic THz lab-on-chip devices for biosensing applications such as the analysis of proteins and detection of circulating tumor cells.

ACKNOWLEDGMENTS

Z.M. acknowledges the National University of Singapore Graduate School for Integrative Sciences and Engineering (NGS) scholarship. S.A.M. acknowledges the Royal Society, the Leverhulme Trust, and the Lee-Lucas Chair for funding. P.A.H. acknowledges funding from a Marie Sklodowska-Curie Fellowship. This work was financially supported by Grant No. EP/M001121/1 from the UK's Engineering and Physical Science Research Council (EPSRC) and partially supported by EDB,

Singapore with Grant No. S15-1322-IAF OSTIn-SIAG. Data supporting this publication can be obtained upon request from teracell@imperial.ac.uk.

[1] P. H. Siegel, "Terahertz technology in biology and medicine," IEEE Trans. Microwave Theory Tech. **52**, 2438–2447 (2004).
[2] D. Mittleman, *Sensing With Terahertz Radiation* (Springer, 2013), Vol. 85.
[3] D. Jahn, A. Soltani, J. C. Balzer, M. Koch, and W. Withayachumnankul, "Fabry-Perot interferometer for sensing polar liquids at terahertz frequencies," J. Appl. Phys. **121**, 204502 (2017).
[4] Z. Ma, S. M. Hanham, P. Albella, B. Ng, H. T. Lu, Y. Gong, S. A. Maier, and M. Hong, "Terahertz all-dielectric magnetic mirror metasurfaces," ACS Photonics **3**, 1010–1018 (2016).
[5] S. J. Park, J. T. Hong, S. J. Choi, H. S. Kim, W. K. Park, S. T. Han, J. Y. Park, S. Lee, D. S. Kim, and Y. H. Ahn, "Detection of microorganisms using terahertz metamaterials," Sci. Rep. **4**, 4988 (2014).
[6] X. Hu, G. Xu, L. Wen, H. Wang, Y. Zhao, Y. Zhang, D. R. S. Cumming, and Q. Chen, "Metamaterial absorber integrated microfluidic terahertz sensors," Laser Photonics Rev. **10**, 962–969 (2016).
[7] S. Park, S. Yoon, and Y. Ahn, "Dielectric constant measurements of thin films and liquids using terahertz metamaterials," RSC Adv. **6**, 69381–69386 (2016).
[8] M. Chen, L. Singh, N. Xu, R. Singh, W. Zhang, and L. Xie, "Terahertz sensing of highly absorptive water-methanol mixtures with multiple resonances in metamaterials," Opt. Express **25**, 14089–14097 (2017).
[9] S. A. Maier, *Plasmonics: Fundamentals and Applications* (Springer Science & Business Media, 2007).
[10] J. B. Pendry, L. Martin-Moreno, and F. J. Garcia-Vidal, "Mimicking surface plasmons with structured surfaces," Science **305**, 847–848 (2004).
[11] F. J. García-Vidal, L. Martín-Moreno, and J. B. Pendry, "Surfaces with holes in them: New plasmonic metamaterials," J. Opt. A: Pure Appl. Opt. **7**, S97–S101 (2005).
[12] A. P. Hibbins, B. R. Evans, and J. R. Sambles, "Experimental verification of designer surface plasmons," Science **308**, 670–672 (2005).
[13] C. R. Williams, S. R. Andrews, S. A. Maier, A. I. Fernández-Domínguez, L. Martín-Moreno, and F. J. García-Vidal, "Highly confined guiding of terahertz surface plasmon polaritons on structured metal surfaces," Nat. Photonics **2**, 175–179 (2008).
[14] A. P. Hibbins, E. Hendry, M. J. Lockyear, and J. R. Sambles, "Prism coupling to 'designer' surface plasmons," Opt. Express **16**, 20441 (2008).
[15] M. A. Kats, D. Woolf, R. Blanchard, N. Yu, and F. Capasso, "Spoof plasmon analogue of metal-insulator-metal waveguides," Opt. Express **19**, 14860 (2011).
[16] X. Shen, T. Jun, D. Martin-cano, and F. J. Garcia-vidal, "Conformal surface plasmons propagating on ultrathin and flexible films," Proc. Natl. Acad. Sci. U. S. A. **110**, 40 (2012).
[17] H. F. Ma, X. Shen, Q. Cheng, W. X. Jiang, and T. J. Cui, "Broadband and high-efficiency conversion from guided waves to spoof surface plasmon polaritons," Laser Photonics Rev. **8**, 146–151 (2014).
[18] Y. J. Zhou, Q. Jiang, and T. J. Cui, "Bidirectional bending splitter of designer surface plasmons," Appl. Phys. Lett. **99**, 111904 (2011).
[19] Q. Gan, Z. Fu, Y. J. Ding, and F. J. Bartoli, "Ultrawide-bandwidth slow-light system based on THz plasmonic graded metallic grating structures," Phys. Rev. Lett. **100**, 256803 (2008).
[20] M. Navarro-Cía, M. Beruete, S. Agrafiotis, F. Falcone, M. Sorolla, and S. A. Maier, "Broadband spoof plasmons and subwavelength electromagnetic energy confinement on ultrathin metafilms," Opt. Express **17**, 18184 (2009).
[21] B. C. Pan, H. C. Zhang, and T. J. Cui, "Multilayer transmissions of spoof surface plasmon polaritons for multifunctional applications," Adv. Mater. Technol. **2**, 1600159 (2017).
[22] A. I. Fernández-Domínguez, E. Moreno, L. Martín-Moreno, and F. J. García-Vidal, "Guiding terahertz waves along subwavelength channels," Phys. Rev. B **79**, 233104 (2009).
[23] B. K. Juluri, S.-c. S. Lin, T. R. Walker, L. Jensen, and T. J. Huang, "Propagation of designer surface plasmons in structured conductor surfaces with parabolic gradient index," Opt. Express **17**, 2997 (2009).
[24] Z. Liao, J. Zhao, B. C. Pan, X. P. Shen, and T. J. Cui, "Broadband transition between microstrip line and conformal surface plasmon waveguide," J. Phys. D: Appl. Phys. **47**, 315103 (2014).
[25] A. Kianinejad, Z. N. Chen, and C. W. Qiu, "Design and modeling of spoof surface plasmon modes-based microwave slow-wave transmission line," IEEE Trans. Microwave Theory Tech. **63**, 1817–1825 (2015).
[26] W. Sun, Q. He, S. Sun, and L. Zhou, "High-efficiency surface plasmon meta-couplers: Concept and microwave-regime realizations," Light: Sci. Appl. **5**, e16003 (2016).
[27] P. A. Huidobro, X. Shen, J. Cuerda, E. Moreno, L. Martin-Moreno, F. Garcia-Vidal, T. J. Cui, and J. Pendry, "Magnetic localized surface plasmons," Phys. Rev. X **4**, 021003 (2014).
[28] A. Pors, E. Moreno, L. Martin-Moreno, J. B. Pendry, and F. J. Garcia-Vidal, "Localized spoof plasmons arise while texturing closed surfaces," Phys. Rev. Lett. **108**, 223905 (2012).
[29] T. Low and P. Avouris, "Graphene plasmonics for terahertz to mid-infrared applications," ACS Nano **8**, 1086–1101 (2014).
[30] H. Lu, C. Zeng, Q. Zhang, X. Liu, M. M. Hossain, P. Reineck, and M. Gu, "Graphene-based active slow surface plasmon polaritons," Sci. Rep. **5**, 8443 (2015).
[31] H. Lu, Y. Gong, D. Mao, X. Gan, and J. Zhao, "Strong plasmonic confinement and optical force in phosphorene pairs," Opt. Express **25**, 5255 (2017).
[32] S. Maier, S. Andrews, L. Martín-Moreno, and F. García-Vidal, "Terahertz surface plasmon-polariton propagation and focusing on periodically corrugated metal wires," Phys. Rev. Lett. **97**, 176805 (2006).
[33] E. Moreno, S. G. Rodrigo, S. I. Bozhevolnyi, L. Martín-Moreno, and F. García-Vidal, "Guiding and focusing of electromagnetic fields with wedge plasmon polaritons," Phys. Rev. Lett. **100**, 023901 (2008).
[34] D. Martin-Cano, M. L. Nesterov, A. I. Fernandez-Dominguez, F. J. Garcia-Vidal, L. Martin-Moreno, and E. Moreno, "Domino plasmons for subwavelength terahertz circuitry," Opt. Express **18**, 754–764 (2010).

[35] L. Zhao, X. Zhang, J. Wang, W. Yu, J. Li, H. Su, and X. Shen, "A novel broadband band-pass filter based on spoof surface plasmon polaritons," Sci. Rep. **6**, 36069 (2016).
[36] C. Watts, S. M. Hanham, M. M. Ahmad, M. Adabi, and N. Klein, "Coupled dielectric-split ring microwave resonator for liquid measurements in microfluidic channels at nanoliter volumes," in *European Microwave Week 2016: "Microwaves Everywhere," EuMW 2016-Conference Proceedings; 46th European Microwave Conference, EuMC 2016* (IEEE, 2017), pp. 257–260.
[37] F. Vollmer and S. Arnold, "Whispering-gallery-mode biosensing: Label-free detection down to single molecules," Nat. Methods **5**, 591–596 (2008).
[38] S. M. Hanham, C. Watts, W. J. Otter, S. Lucyszyn, and N. Klein, "Dielectric measurements of nanoliter liquids with a photonic crystal resonator at terahertz frequencies," Appl. Phys. Lett. **107**, 032903 (2015).
[39] A. Densmore, M. Vachon, D.-X. Xu, S. Janz, R. Ma, Y. H. Li, G. Lopinski, A. Delâge, J. Lapointe, C. C. Luebbert, Q. Y. Liu, P. Cheben, and J. H. Schmid, "Silicon photonic wire biosensor array for multiplexed real-time and label-free molecular detection," Opt. Lett. **34**, 3598 (2009).
[40] A. L. Washburn and R. C. Bailey, "Photonics-on-a-chip: Recent advances in integrated waveguides as enabling detection elements for real-world, lab-on-a-chip biosensing applications," Analyst **136**, 227–236 (2011).
[41] J. F. O'Hara, R. Singh, I. Brener, E. Smirnova, J. Han, A. J. Taylor, and W. Zhang, "Thin-film sensing with planar terahertz metamaterials: Sensitivity and limitations," Opt. Express **16**, 1786 (2008).
[42] N. Liu, M. Mesch, T. Weiss, M. Hentschel, and H. Giessen, "Infrared perfect absorber and its application as plasmonic sensor," Nano Lett. **10**, 2342–2348 (2010).
[43] H. Lu, X. Liu, D. Mao, and G. Wang, "Plasmonic nanosensor based on Fano resonance in waveguide-coupled resonators," Opt. Lett. **37**, 3780 (2012).
[44] B. Ng, J. Wu, S. M. Hanham, A. I. Fernández-Domínguez, N. Klein, Y. F. Liew, M. B. H. Breese, M. Hong, and S. A. Maier, "Spoof plasmon surfaces: A novel platform for THz sensing," Adv. Opt. Mater. **1**, 543–548 (2013).
[45] B. Ng, S. M. Hanham, J. Wu, A. I. Ferna, and N. Klein, "Broadband terahertz sensing on spoof plasmon surfaces," ACS Photonics **1**, 1059–1067 (2014).
[46] X. Shi, J. Qin, and Z. Han, "Enhanced terahertz sensing with a coupled comb-shaped spoof surface plasmon waveguide," Opt. Express **25**, 278 (2017).
[47] Y. G. Ma, L. Lan, S. M. Zhong, and C. K. Ong, "Experimental demonstration of subwavelength domino plasmon devices for compact high-frequency circuit," Opt. Express **19**, 21189 (2011).
[48] G. Kumar, S. Li, M. M. Jadidi, and T. E. Murphy, "Terahertz surface plasmon waveguide based on a one-dimensional array of silicon pillars," New J. Phys. **15**, 085031 (2013).
[49] S. Pandey, B. Gupta, and A. Nahata, "Terahertz plasmonic waveguides created via 3D printing," Opt. Express **21**, 24422 (2013).
[50] X. Liu, Y. Feng, B. Zhu, J. Zhao, and T. Jiang, "High-order modes of spoof surface plasmonic wave transmission on thin metal film structure," Opt. Express **21**, 31155 (2013).